Chapter Three

Assessment of Trabecular Bone Anisotropy

3.1 Introduction

The material property of an object is anisotropic if the property differs in character or quantity according to direction. In trabecular bone, it is the mechanical anisotropy that is of interest. Trabecular bone has been shown to be anisotropic in both strength (3, 19, 21) (Figure 3.1) and modulus (9, 19, 21). These findings are consistent with concepts put forward in the 19th century by Meyer and Wolff (4, 6, 29), who observed that trabecular bone architecture was highly influenced by trabecular bone mechanics, implying that trabecular architecture exhibited preferential alignment corresponding to loading stresses. The consequence of this observation is that trabecular bone mechanics is reflected in the trabecular architecture. That is, anisotropy is a consequence of the adaptive response to functional loading (19).

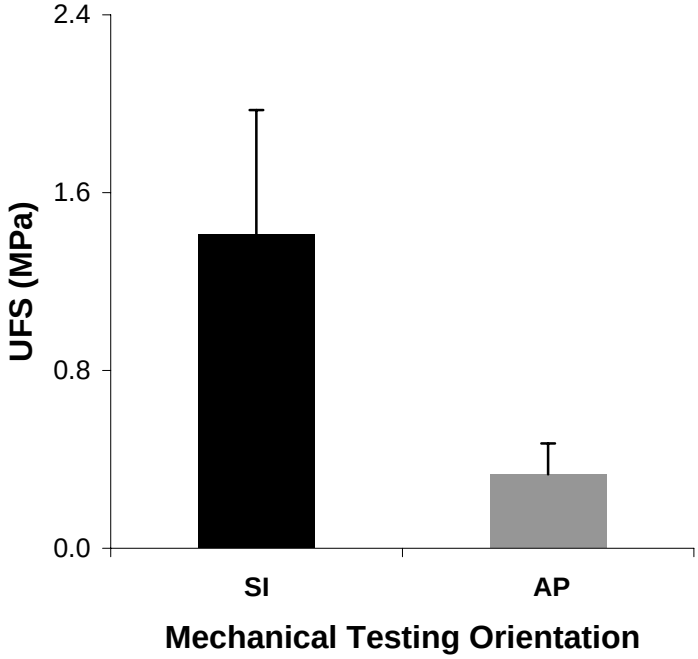

Figure 3.1 Example of mechanical anisotropy within vertebral trabecular bone. Mean and standard deviation of ultimate failure stress (UFS) measured from 24 human vertebral trabecular bone cubes mechanically tested in orthogonal orientations. SI denotes superinferior (n = 12) and AP anteroposterior (n = 12) mechanical testing orientation.

Whitehouse (1974) (28) was the first investigator to quantify the principal structural direction and anisotropy of trabecular bone from histological sections. Using the mean intercept length (MIL) (Section 3.2), Whitehouse (1974) found that an ellipse fit to the polar plot of MIL data described the data well (28). The ratio of major to minor axis of this ellipse would then be representative of the structural anisotropy (16, 19, 28). Using this as a foundation, Harrigan and Mann (1984) described a method for determining the three dimensional anisotropy tensor in orthotropic materials by measuring the MIL in three mutually perpendicular planes and recognizing the result as a second rank tensor defining an ellipsoid (16).

The link between structural anisotropy and mechanical properties of a material was made by Cowin (1985) (5). Cowin (1985) (5) defined the term “fabric tensor” as a measure of local structural anisotropy and classified it as the inverse of the MIL tensor (5, 19). His generalization was able to link the fabric tensor to the anisotropic elastic properties of a material. Using this theory, the degree of structural anisotropy was quantified using the ratios of the eigenvalues of the fabric tensor. Many investigations have explored the relationship between fabric-derived measures of structural anisotropy and the mechanical properties of trabecular bone (7, 14, 17, 27).

While the MIL and the associated fabric tensor is the standard quantitative descriptor of trabecular structural anisotropy (2, 16, 22, 28), other measures have also been developed and tested on trabecular bone. The line fraction deviation (LFD), star length distribution (SLD) and star volume distribution (SVD) are three popular alternatives (12, 22, 25). In this thesis, only the MIL and LFD will be considered. The SLD and SVD are described in this chapter for completeness.

To demonstrate measurement of anisotropy using the various descriptors, an example trabecular bone image will be used in the sections to follow (Figure 3.2).

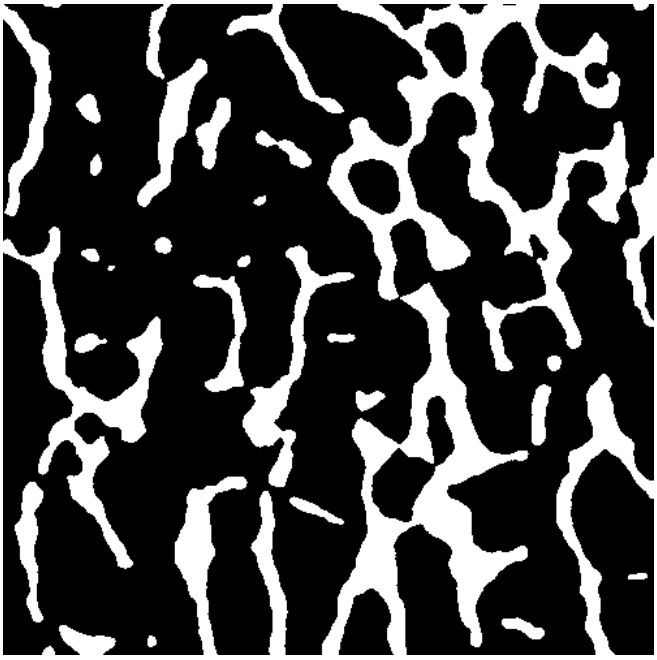

Figure 3.2 Coronal µCT tomograph taken from a trabecular bone cube dataset of an L2 vertebral from a 33 year old female with bone volume fraction, BV/TV = 23.7 %. This image will be used to demonstrate the measurement of anisotropy using the various anisotropy descriptors.

3.2 Mean Intercept Length

The MIL is the mean distance between two bone/ marrow interfaces (22, 25). The fundamental principles of this technique arise from the field of stereology and the underlying mathematics (integral geometry) may be viewed as a variation of Buffon's needle problem (18, 24).

The computation of the MIL consists of the sampling of intersections between a sampling grid (Section 3.6) and the bone/ marrow interface as a function of the grid's orientation, ϕ (22). The MIL can be expressed as

$$\mathrm{MIL}(\phi) = \frac{L}{I(\phi)}, 0^{o} \leq \phi < 180^{o} \quad , \qquad 3.1$$

where MIL(ϕ) is the mean intercept length component at orientation ϕ, L is the total length of the sampling grid and I(ϕ) is the number of intercepts sampled at orientation ϕ (Figure 3.3).

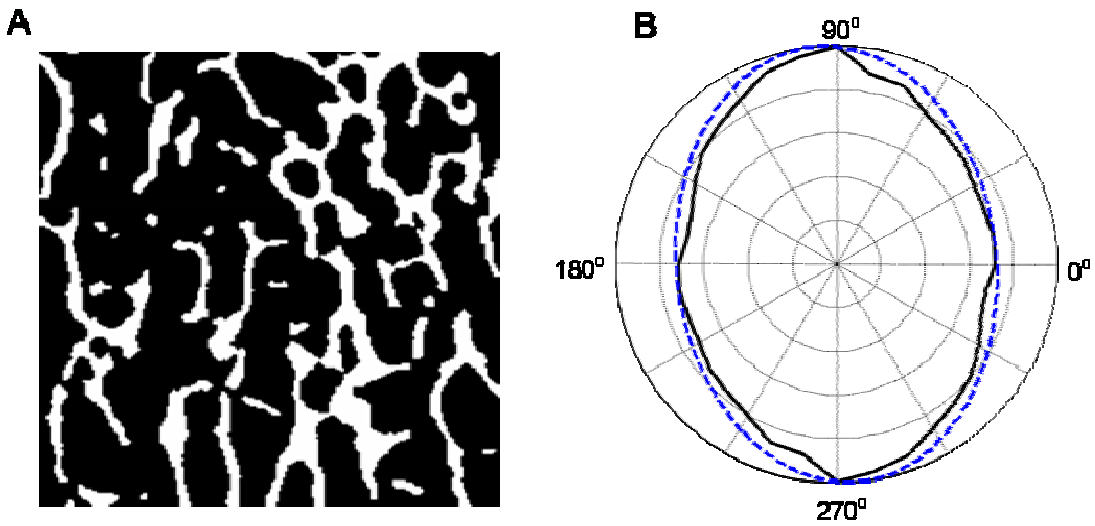

Figure 3.3 Example of MIL based anisotropy measurement from a µCT tomograph of human trabecular bone. [A] Binary µCT tomograph of human trabecular bone, [B] Values for $\mathrm{MIL}(\phi)$ for $\phi = \frac{\pi}{18}n$, for n = 1,2,…,18 (solid black) and the best-fitting ellipse (dashed blue). The polar plot is shown in degrees and data been have been normalised with respect to the maximum anisotropy value for illustration purposes.

3.3 Line Fraction Deviation

The line fraction deviation (LFD) was introduced by Geraets *et al* (12) as an index of orientation applied to segmented radiographic images of trabecular networks. The LFD is the standard deviation of the fraction of trabecular bone pixels within a grid (11, 12). In the segmented image, if the trabecular bone pattern aligns with respect to the grid, a larger standard deviation will be recorded compared to when the trabecular bone pattern does not align with respect to the grid (11, 13). This, in effect, captures architectural anisotropy information (Figures 3.4 and 3.5).

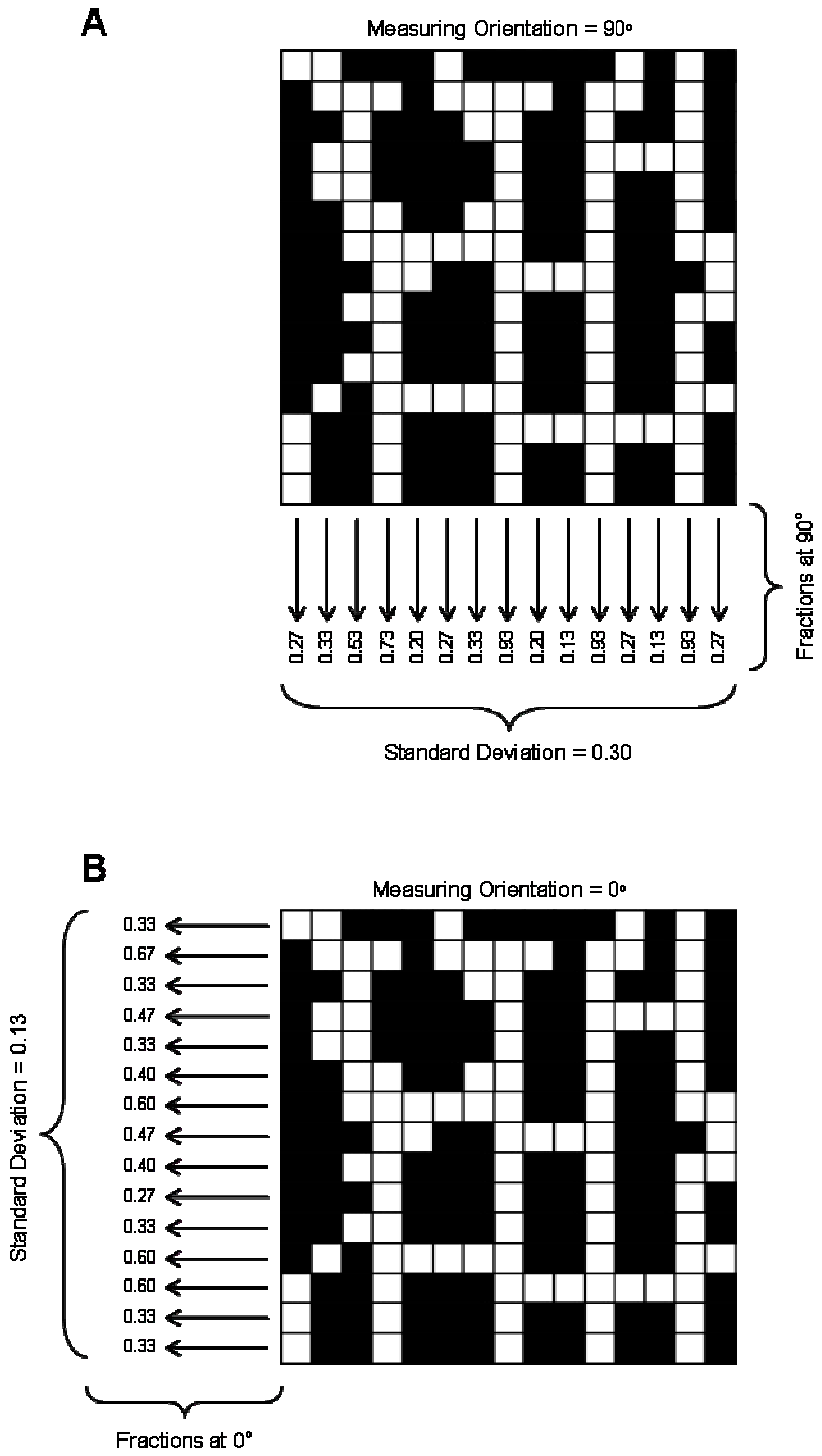

Figure 3.4 Measurement of the LFD depicted graphically. With the measuring orientation set at 90°, up and down the page [A], the LFD is greater (LFD_{90} = 0.30) than that when the measuring orientation is at 0°, across the page [B], where LFD_0 = 0.13. This indicates greater structural alignment at 90° than at 0°.

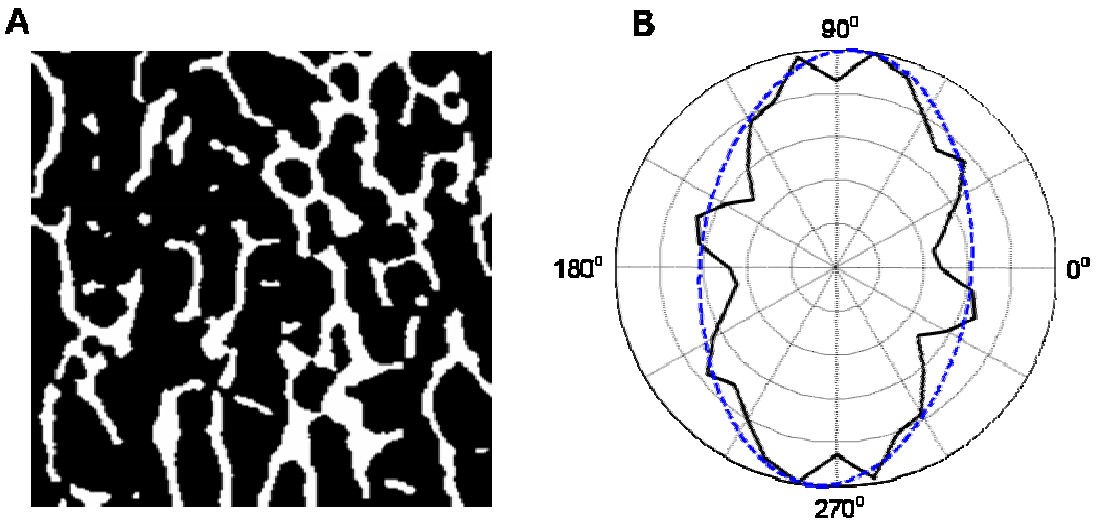

Figure 3.5 Example of LFD based anisotropy measurement from a µCT tomograph of human trabecular bone. [A] Binary µCT tomograph of human trabecular bone, [B] Values for LFD(ϕ) for $\phi = \frac{\pi}{18}n$, for n = 1,2,…,18 (solid black) and the best-fitting ellipse (dashed blue). The polar plot is shown in degrees and data have been have been normalised with respect to the maximum anisotropy value for illustration purposes.

3.4 Star Volume Distribution

The star volume distribution (SVD) technique was introduced by Cruz-Orive *et al* (8) and is closely related to the star volume defined by Gundersen & Jense (13, 15). The SVD describes the typical distribution of trabecular bone around a typical point in a trabecula. The SVD is the mean volume of a trabecula seen unobstructed from a random point within the trabecula, evaluated as a function of orientation. If sampling at random points is replaced by sampling on a grid (25), the SVD can be expressed as

$$SVD(\phi) = \frac{\pi}{3} \frac{\sum_{i=1}^{n} (Li(\phi))^4}{\sum_{i=1}^{n} (Li(\phi))}, 0^o \leq \phi < 180^o \quad , \qquad 3.2$$

where SVD(ϕ) is the star volume component at orientation ϕ and Li is the length of the intersection i of a grid line with a trabecular structure (Figure 3.6).

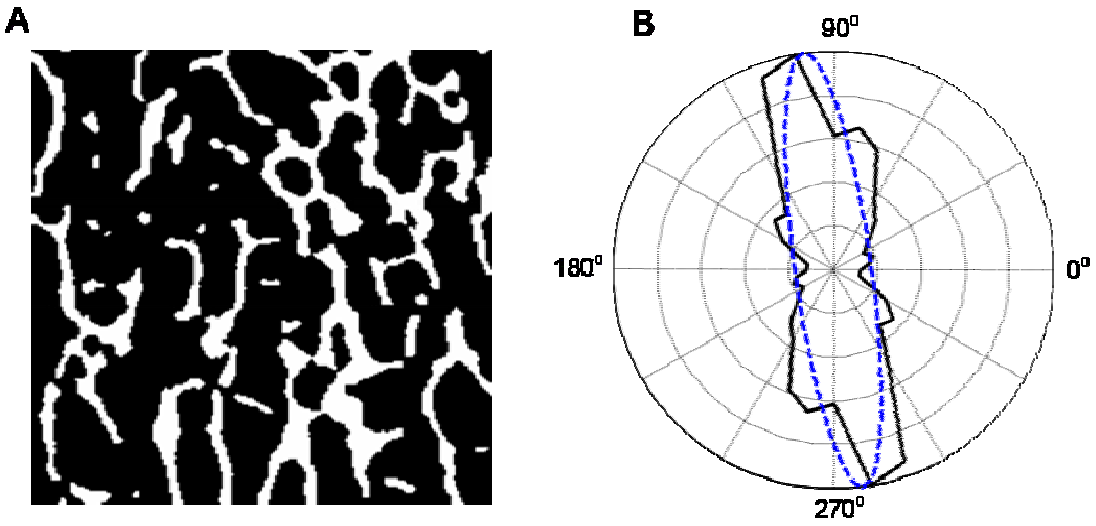

Figure 3.6 Example of SVD based anisotropy measurement from a µCT tomograph of human trabecular bone. [A] Binary µCT tomograph of human trabecular bone, [B] Values for $\mathrm{SVD}(\phi)$ for $\phi = \frac{\pi}{18}n$, for n = 1,2,…,18 (solid black) and the best-fitting ellipse (dashed blue). The polar plot is shown in degrees and data have been have been normalised with respect to the maximum anisotropy value for illustration purposes.

3.5 Star Length Distribution

The star length distribution (SLD) was introduced by Odgaard *et al* (23) as a slight modification on the SVD (20, 22, 25). SLD employs a similar computational procedure as the SVD with the addition of weighting by the observed intersection length. If sampling at random points is replaced by sampling on a grid (25), the SLD can be expressed as

$$SLD(\phi) = \frac{\sum_{i=1}^{n} (L_i(\phi))^2}{\sum_{i=1}^{n} Li(\phi)}, 0^o \leq \phi < 180^o, \qquad 3.3$$

where SLD(ϕ) is the star length component at orientation ϕ and L_i is the length of the intersection *i* of a grid line with the trabecular structure (Figure 3.7).

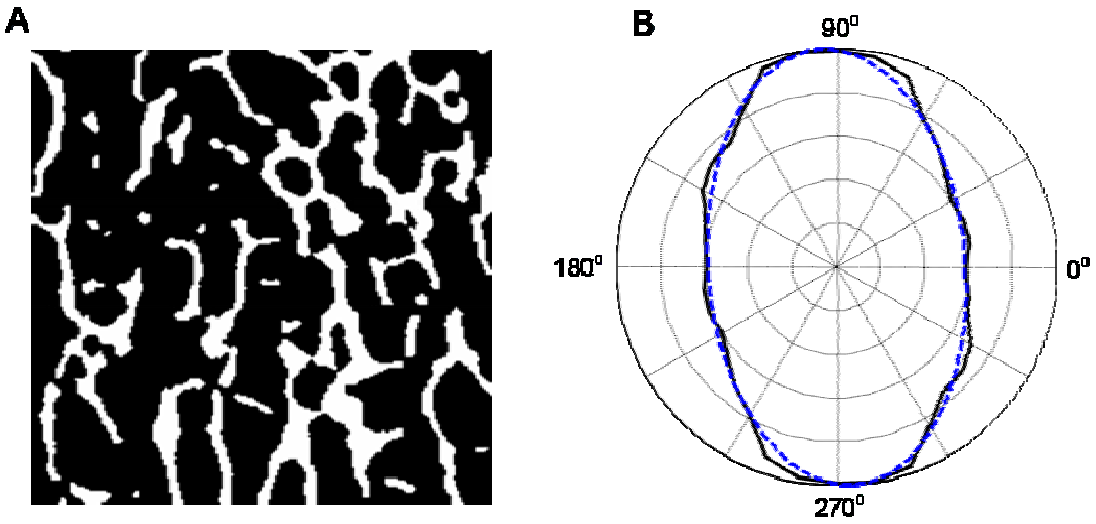

Figure 3.7 Example of SLD based anisotropy measurement from a µCT tomograph of human trabecular bone. [A] Binary µCT tomograph of human trabecular bone, [B] Values for $\mathrm{SLD}(\phi)$ for $\phi = \frac{\pi}{18}n$, for n = 1,2,…,18 (solid black) and the best-fitting ellipse (dashed blue). The polar plot is shown in degrees and data have been have been normalised with respect to the maximum anisotropy value for illustration purposes.

3.6 Technical Aspects of Anisotropy Measurement

In order to measure anisotropy from a square image of size $\ell \times \ell$, a square grid centered on the image was used. To ensure overlap within the image, the square grid had to fit completely within the image at all orientations. To achieve this the length of the sides of the square gird had to be of size $m = \frac{\ell}{\sqrt{2}}$. This is equivalent to selecting a circular region of interest that fits with in a square image (Figure 3.8).

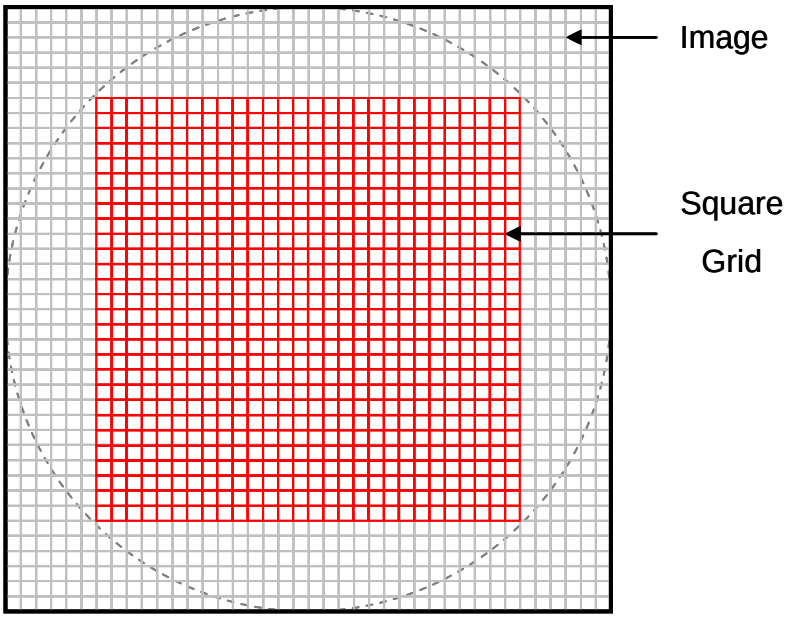

Figure 3.8 Example illustrating the square grid constructed inside the image. When rotated within the image, the square grid inscribes a circular region of interest.

For all anisotropy measures described, indices of anisotropy measured at orientation ϕ are the same as the values measured at orientation $\phi \pm n\pi$ for any n.

3.7 Two Dimensional Analyses

Anisotropy measurements can be made on 2D tomographic images (Figures 3.3, 3.5, 3.6 and 3.7). This form of analysis is directly associated with histomorphometric analyses carried out on histology sections. 2D analyses can be carried out on single images or multiple images. Extrapolating 2D information to 3D requires that the specimen being investigated be sampled over all possible orientations in space. However, without access to the 3D structure, it is impossible to sample over all possible directions non-destructively. To overcome this issue it is possible to sample specimens in three mutually perpendicular directions.

Anisotropy in a given plane can be estimated as the average anisotropy over a number of sections in that plane. For example, the average sagittal anisotropy of a cube of vertebral trabecular bone can be measured as the average anisotropy over a number of anisotropy measurements made in the sagittal plane (Figure 3.9).

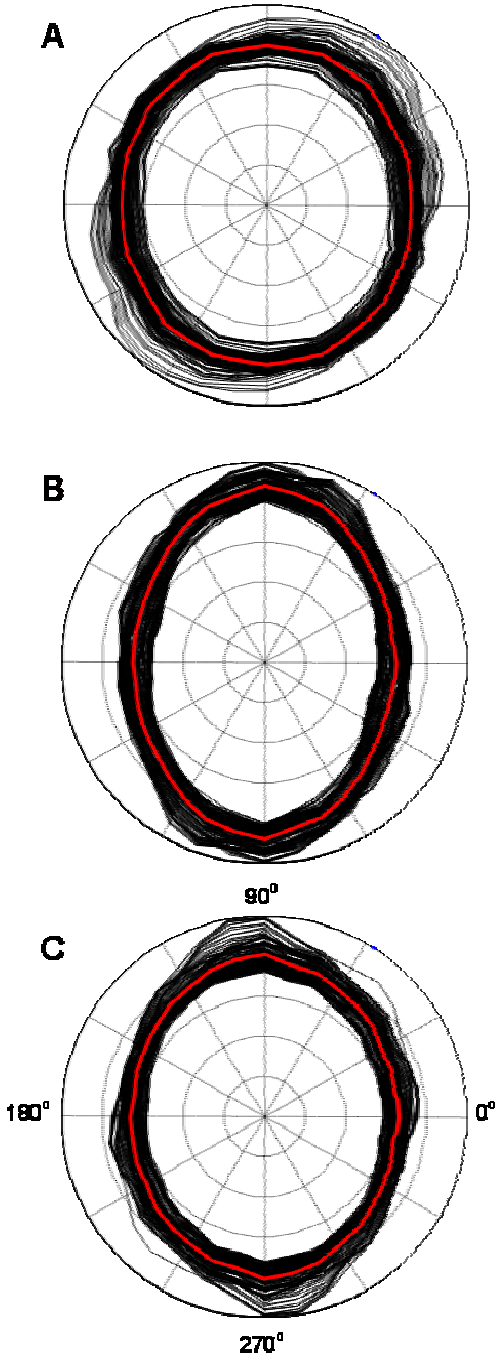

Figure 3.9 Measurement of the MIL in three orthogonal planes, [A] axial, [B] coronal and [C] sagittal, from a cube of human trabecular bone. MIL based anisotropy from a number of 2D tomographs have been overlaid on top of each other and are shown in black, while the mean anisotropy is shown in red. Data have been have been normalised with respect to the maximum anisotropy value for illustration purposes.

3.7.1 Two Dimensional Degree of Anisotropy

To determine the degree of anisotropy (DA) from the 2D anisotropy data, $A(\phi_n)$, the quantity $A(\phi_n)$ is typically computed for $\frac{\pi(n-1)}{18}$ for $n = 1,\ldots,18$. Anisotropy can then be visualized by plotting the points (x_n, y_n) with $x_n = \cos(A(\phi_n))$ and $y_n = \sin(A(\phi_n))$. The value of the DA is then the ratio of the eigenvalues of the 2×2 matrix, X^TX, where $X(n,1) = x_n - \bar{x}$, $X(n,2) = y_n - \bar{y}$ and X^T is the transpose of X. Since the eigenvectors and eigenvalues of X^TX determine the orientation and lengths of the major and minor axis of the ellipse that best fits the points (x_n, y_n), this definition of DA is tantamount to finding the ellipse of equivalent anisotropy (1).

In the examples shown (Figure 3.9) the DA was found to be 1.06, 1.29 and 1.15 for the axial, coronal and sagittal planes, respectively.

Ellipse versus Raw Anisotropy Data

While fitting an ellipse to MIL data has a direct relationship to the material's mechanical properties (as demonstrated by the work of Harrigan and Mann (1984) and Cowin (1985) (5, 16, 28)), the fitting of ellipses to other anisotropy measures does not have the same fundamental reasoning. The LFD (and the LPD described in the Chapter 6) are more sensitive to architectural variations and as such are able to capture more than just the primary and secondary axes of alignment (10, 11). In these more sensitive techniques one might consider measuring the maximum and minimum radii of the anisotropy data. These maxima and minima would effectively correspond to the maximum and minimum structural property measured by the given technique. For example, in the case of the LFD, the maxima and minima are representative of the maximum and minimum line fraction deviation, a surrogate of structural alignment (Figures 3.10 and 3.11). However, measurement of maxima and minima, being based on single data points, are susceptible to error. For example, a noisy element in an image may trigger a false maxima or minima, leading to incorrect representation of the structural anisotropy.

As such, a method for capturing the average anisotropy information from such data would be a better alternative. Fitting of an ellipse to data generated from measures such as the LFD has the affect of capturing the general trend or average of the LFD data. Hence, the procedure used for finding the best-fitting ellipse to the MIL anisotropy data (described above) will also be employed for computing the DA from other measures of anisotropy.

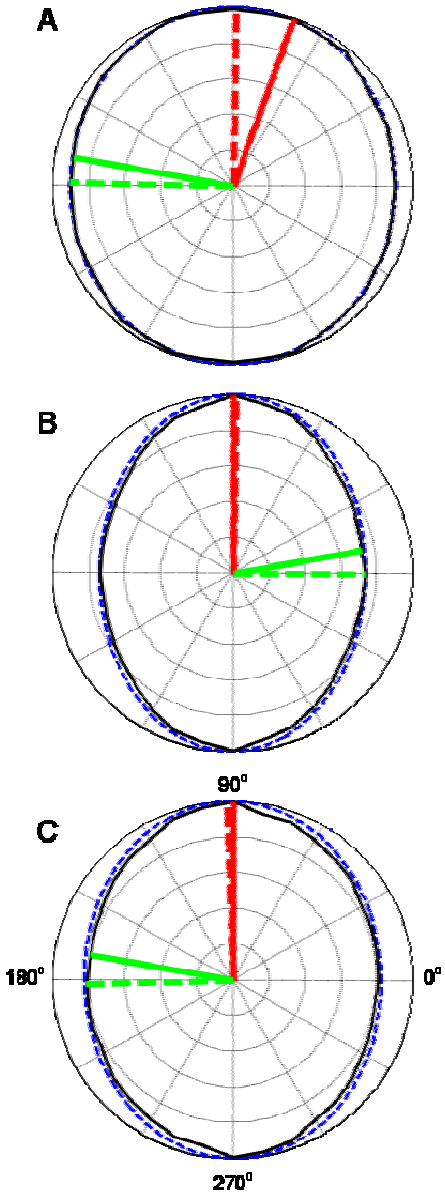

Figure 3.10 Example illustrating the relationship between maximum and minimum radii with the resulting best-fitting ellipse. Anisotropy calculated in the [A] axial, [B] coronal and [C] sagittal planes. Mean MIL anisotropy shown in solid black, best-fitting ellipse shown in dashed blue. The maximum radius of the mean anisotropy data is shown in solid red, the minimum radius of the mean anisotropy data is show in solid green. The major axis of the best-fitting ellipse is shown in dashed red, the minor axis of the best-fitting ellipse is shown in dashed green. Note that for the MIL the maximum and minimum radii essentially correspond to the major and minor axes of the best-fitting ellipse. Data have been have been normalised with respect to the maximum anisotropy value for illustration purposes.

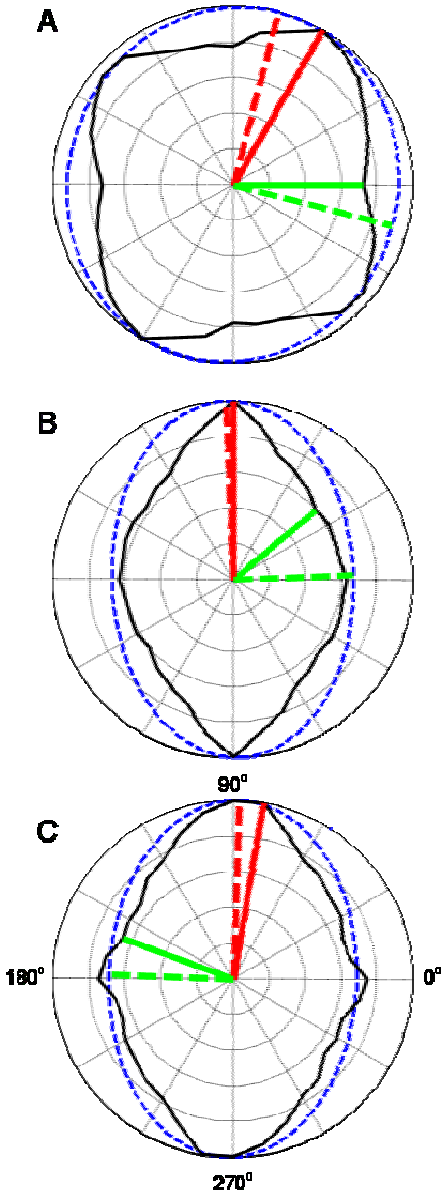

Figure 3.11 Example illustrating the relationship between maximum and minimum radii with the resulting best-fitting ellipse. Anisotropy calculated in the [A] axial, [B] coronal and [C] sagittal planes. Mean LFD anisotropy shown in solid black, best-fitting ellipse shown in dashed blue. The maximum radius of the mean anisotropy data is shown in solid red, the minimum radius of the mean anisotropy data is show in solid green. The major axis of the best-fitting ellipse is shown in dashed red, the minor axis of the best-fitting ellipse is shown in dashed green. Note that for the LFD the maximum and minimum radii do not correspond to the major and minor axes of the best-fitting ellipse, however the ellipse does provide information regarding the general trend of the data. Data have been have been normalised with respect to the maximum anisotropy value for illustration purposes.

3.7.2 Pseudo Three Dimensional Analyses

A number of authors have shown that the MIL, when plotted in polar form, generates an ellipse (16, 28). Harrigan and Mann (1984) (16) made the generalization that the resultant ellipses from three orthogonal planes correspond to the projections of an ellipsoid on the section planes. Hence, 2D measurements of the MIL made in three orthogonal directions can be used to generate an ellipsoid representing the 3D anisotropy. A number of studies have shown this to be a reliable and effective technique (14, 26, 28).

Since this thesis is focused on the relationship between trabecular bone structure and projected (or x-ray) information, direct 2D anisotropy information, as described in section 3.7.1 will be used. Pseudo three dimensional analyses will not be considered.

3.8 Three Dimensional Analysis

With the advent of non-destructive imaging modalities such as μCT, the possibility of performing direct 3D measurement of anisotropy has become a reality. The MIL is one of the most commonly used measures of anisotropy and as such was one of the initial measures to migrate to direct 3D assessment. Analogous to the 2D technique, 3D MIL measures the number of intercepts between a set of test lines and the volume of interest. 3D MIL is computed using a series of lines in a 3D volume containing binarised objects. Similar to the 2D equivalent (Section 3.2), the length of the test lines through the volume is normalised by the number of intersections between the test lines and the bone phase. The grid of lines must be sent through the volume over a large number of 3D angles and the resulting MIL at each angle is calculated as the average for all the lines of the grid. A spherical volume of interest is defined within which the MIL analysis is carried out to ensure that the same region of the volume is assessed for all angles (22).

Similar to the processes described above, the best-fitting ellipsoid to the 3D MIL data is calculated. From this ellipsoid, the tensor describing the anisotropy ellipsoid is obtained and analyses carried out to determine the eigenvectors and eigenvalues. Analogous to the 2D MIL, the degree of anisotropy (DA) is calculated as the ratio of maximum to minimum eigenvalue from the resulting MIL ellipsoid (14, 22).

While 3D measures of anisotropy do exist for the LFD (10) and the other measures described in this chapter (22, 25), only the 3D MIL will be considered in subsequent analyses. This is due to the fact that the 3D MIL is the most widely recognized and studied 3D measure of anisotropy and directly related to the work in this thesis.

References

1. Badiei, A., Bottema, M.J. and Fazzalari, N.L. Expected and Observed Changes to Architectural Parameters of Trabecular Bone with Aging A Comparison of Measurement Techniques. Digital Image Computing: Technqiues and Applications, 2005. DICTA ' 05. Proceedings:491 - 497; 2005.
2. Chappard, C., Brunet-Imbault, B., Lemineur, G., Giraudeau, B., Basillais, A., Harba, R., and Benhamou, C. L. Anisotropy changes in post-menopausal osteoporosis: characterization by a new index applied to trabecular bone radiographic images. Osteoporos Int; 2005.
3. Ciarelli, M. J., Goldstein, S. A., Kuhn, J. L., Cody, D. D., and Brown, M. B. Evaluation of orthogonal mechanical properties and density of human trabecular bone from the major metaphyseal regions with materials testing and computed tomography. J Orthop Res 9:674-82; 1991.
4. Cowin, S. C. The False Premise in Wolff's Law. In: S. C. Cowin (ed.), Bone Mechanics Handbook, pp. 30/1 - 30/15. New York: CRC Press; 2001.
5. Cowin, S. C. The Relationship Between the Elasticity Tensor and the Fabric Tensor. Mechanics of Materials 4:137 - 147; 1985.
6. Cowin, S. C. Wolff's law of trabecular architecture at remodeling equilibrium. J Biomech Eng 108:83-8; 1986.
7. Cowin, S. C., and Turner, C. H. On the relationship between the orthotropic Young's moduli and fabric. J Biomech 25:1493-4; 1992.
8. Cruz-Orive, L. M., Karlsson, L. M., Larsen, S. E., and Wainschtein, F. Characterizing Anisotropy: A New Concept. Micron and Microscopica Acta 23:75 - 76; 1992.
9. Galante, J., Rostoker, W., and Ray, R. D. Physical properties of trabecular bone. Calcif Tissue Res 5:236-46; 1970.
10. Geraets, W., van Ruijven, L., Verheij, J., van Eijden, T., and van der Stelt, P. A sensitive method for measuring spatial orientation in bone structures. Dentomaxillofac Radiol 35:319-25; 2006.
11. Geraets, W. G. Comparison of two methods for measuring orientation. Bone 23:383-8; 1998.
12. Geraets, W. G., Van der Stelt, P. F., Lips, P., Elders, P. J., Van Ginkel, F. C., and Burger, E. H. Orientation of the trabecular pattern of the distal radius around the menopause. J Biomech 30:363-70; 1997.
13. Geraets, W. G., Van der Stelt, P. F., Netelenbos, C. J., and Elders, P. J. A new method for automatic recognition of the radiographic trabecular pattern. J Bone Miner Res 5:227-33; 1990.
14. Goulet, R. W., Goldstein, S. A., Ciarelli, M. J., Kuhn, J. L., Brown, M. B., and Feldkamp, L. A. The relationship between the structural and orthogonal compressive properties of trabecular bone. J Biomech 27:375-89; 1994.
15. Gundersen, H. J., and Jensen, E. B. Stereological Estimation of the Volume-Weighted Mean Volume of Arbitrary Particles Observed on Random Sections. Journal Of Microscopy 138:127 - 142; 1985.
16. Harrigan, T. P., and Mann, R. W. Characterization of Microsturctural Anisotropy in Orthotropic Materials Using a Second Rank Tensor. Journal of Material Science 19:761 - 767; 1984.
17. Kabel, J., van Rietbergen, B., Odgaard, A., and Huiskes, R. Constitutive relationships of fabric, density, and elastic properties in cancellous bone architecture. Bone 25:481-6; 1999.
18. Kanatani, K. Measurement of Particle Orientation Distribution by a Stereological Method. Part. Charact. 2:31 - 37; 1985.
19. Keaveny, T. M., Morgan, E. F., Niebur, G. L., and Yeh, O. C. Biomechanics of trabecular bone. Annu Rev Biomed Eng 3:307-33; 2001.
20. Ketcham, R. A., and Ryan, T. M. Quantification and Visualization of Anisotropy in Trabecular Bone. Journal Of Microscopy 213:158 - 171; 2004.
21. Mosekilde, L., and Danielsen, C. C. Biomechanical competence of vertebral trabecular bone in relation to ash density and age in normal individuals. Bone 8:79-85; 1987.
22. Odgaard, A. Three-dimensional methods for quantification of cancellous bone architecture. Bone 20:315-28; 1997.
23. Odgaard, A., Kabel, J., van Rietbergen, B., Dalstra, M., and Huiskes, R. Fabric and elastic principal directions of cancellous bone are closely related. J Biomech 30:487-95; 1997.
24. Russ, J. C., and Dehoff, R. T. Practical Stereology. New York: Plenum Publishers; 2000.
25. Smit, T. H., Schneider, E., and Odgaard, A. Star length distribution: a volume-based concept for the characterization of structural anisotropy. J Microsc 191 (Pt 3):249-57; 1998.
26. Snyder, B. D. Anisotropic Structure-Property Relations for Trabecular Bone. Bioengineering, pp. 260: Univeristy of Pennsylvania; 1991.
27. Turner, C. H., Cowin, S. C., Rho, J. Y., Ashman, R. B., and Rice, J. C. The fabric dependence of the orthotropic elastic constants of cancellous bone. J Biomech 23:549-61; 1990.
28. Whitehouse, W. J. The quantitative morphology of anisotropic trabecular bone. J Microsc 101 Pt 2:153-68; 1974.
29. Wolff, J. D. Das Gesetz der Transformation der Knochen. Berlin, A. Hirschwald. 1892.

Chapter Four

Mechanical Anisotropy of Vertebral Trabecular Bone

4.1 Introduction

Trabecular structure has evolved to provide a high level of functionality. Bone strength, the ability of the bone to withstand fracture, is obviously an important property of bone. However, fractures and bone damage are inevitable and so desirable properties of bone are its ability to remain functional and repair subsequent damage. Vertebral fractures, commonly associated with osteoporosis, ranging from mild wedge compressions to severe crush fractures are believed to be silent in two-thirds of women (19). This indicates that despite structural failure, vertebra remain in a loaded environment where they transmit functional loads through the spine (11). Further evidence comes from callus formation (11) on individual trabeculae across a number of anatomical sites (6, 13). This indicates that the trabecular structure can sustain damage, undergo repair and still maintain function. The question of how trabecular structure is able to maintain mechanical integrity and function after sustaining damage remains largely unanswered.

A number of studies have attempted to address this question. Fyhrie and Schaffler (1994) reported a qualitative assessment of the mechanisms of failure in human vertebral trabecular bone when loaded in the anatomical superoinferior direction (4). Their observations indicate that when large compressive strains are applied to vertebral trabecular bone, the majority of the damage is limited to elements transverse to the loading direction, with damage to vertical elements being mainly microscopic “internal matrix microdamage”. They did not investigate whether the failure mechanisms during transverse loading would have similar outcomes. Fazzalari *et al* (1998) carried out monotonic mechanical testing on intertrochanteric biopsies from the proximal femur and evaluated the microdamage post-failure (3). Their observations showed a link between age, structural microdamage and mechanical integrity. However, the relationship between the principal axis of loading of the proximal femur and the spatial arrangement of the structure of trabecular bone is much more complex when compared to that of the vertebral body. Therefore, while not directly

applicable to the vertebral body, their study does provide insight into some of the general failure mechanisms of trabecular bone. Similarly, investigations by Keaveny *et al* on post-yield mechanics of bovine tibial (11) and human vertebral trabecular bone (12) and Kopperdahl *et al* (2000) on whole vertebral bodies (14) provided further insight into the failure mechanisms of trabecular bone. These overload-release-reload investigations highlighted many aspects of trabecular bone damage behavior, including observations that indicate post-yield behavior may be dominated by the ultra-structural material properties of trabecular bone (11, 12, 14). These studies provided information on the damage behavior of trabecular bone after overloading in the principal anatomical loading direction. The authors did not investigate whether off-axis (transverse) loading would result in similar observations.

While the aforementioned studies focus on the principal anatomical loading direction, the structural and mechanical anisotropy is largely overlooked. A number of studies have considered monotonic failure mechanics of vertebral trabecular bone in orthogonal directions (5, 17, 18). These studies focused on the relative difference between failure loads in orthogonal directions and not the influence of failure mechanics orthogonal to initial failure. With findings by Mosekilde *et al* (1985) illustrating that the vertebral strength anisotropy index (ratio of longitudinal to transverse strength) increases with age (18), the question regarding the mechanical relationship between longitudinal and transverse elements, and the consequences of that relationship on global mechanical integrity arises.

The aim of this chapter was to investigate mechanical anisotropy within vertebral trabecular bone and the effect of initial overload on the mechanical integrity of trabecular bone orthogonal to the initial overload. Specifically, superoinferior and anteroposterior mechanical properties were measured before and after overload to investigate the role of mechanical anisotropy in vertebral trabecular bone.

4.2 Materials and Methods

The study included vertebral bodies from 12 cases (9 males and 3 females) with a median age of 68 and age range 53 – 83. At postmortem examination, the T12/L1 vertebral bodies from 5 cases (4 males and 1 female) and the L4/L5 vertebral bodies from the remaining 7 (5 males and 2 females) were collected.

All vertebral bodies were wrapped in saline soaked gauze and stored at -30^{o}C immediately after collection. A cube of trabecular bone 10x10x10 mm was obtained from the centrum of each vertebral body by cutting through the frozen vertebral bodies (Chapter 2, Section 2.1.1). Exact dimensions of cubes were measured using digital calipers (Chapter 2, Section 2.2.1).

Cubes from each T12/L1 and L4/L5 pair were assigned to either superoinferior (SI) or anteroposterior (AP) mechanical testing groups using a random selection process; a random number generator (Matlab, The Mathworks) provided a number between 0 and 1 and cubes assigned to SI for numbers greater than 0.5 and AP for less than or equal to 0.5. Since cube pairs were collected from adjacent vertebral bodies, once one of the pair was assigned to a SI or AP group the adjacent cube was automatically assigned to the other group. Final assignments resulted in 3, 2, 4 and 3 (T12, L1, L4 and L5, respectively) cubes assigned to SI and 2, 3, 3 and 4 (T12, L1, L4 and L5, respectively) cubes assigned to AP.

Trabecular bone cubes were then imaged using a Skyscan 1072 x-ray microcomputed tomography (μCT) system (Chapter 2, Section 2.2.3). Tomographic images obtained from scanning were binarised and a component-labeling routine used to remove any unconnected components (Chapter 2, Section 2.2.3). The trabecular structure was analyzed to obtain global average architectural parameters. Standard model-independent 3D algorithms were employed to calculate the bone volume fraction (BV/TV [%]), specific surface (BS/BV [mm^2/mm^3]), total surface (BS/TV [mm^2/mm^3]), trabecular thickness (Tb.Th [μm]), trabecular separation (Tb.Sp [μm]), trabecular number (Tb.N [/mm]), degree of anisotropy (DA), trabecular bone pattern factor (TBPf [/mm]), structure model index (SMI) and connectivity density (Conn.D [$/mm^3$]) (Chapter 2, Section 2.2.3). All parameters were computed using CTAn software provided by the manufacturer of the μCT system. To ensure the principal trabecular orientation of cubes corresponded to the anatomical trabecular alignment, principal orientation within each cube was measured (mean ± standard deviation) using custom written software (Matlab, The Mathworks) for both coronal ($86^o \pm 19^o$) and sagittal ($86^o \pm 9^o$) planes (Chapter 3, Section 3.2).

All mechanical testing was carried out on a universal testing machine controlled by a personal computer and custom designed software (Chapter 2, Section 2.2.5). All samples were tested to 10% apparent strain by uni-axial compression according to their SI or AP allocation. Thus, cubes assigned to SI were positioned such that anatomical superoinferior was parallel to the load train, while cubes assigned to AP were positioned such that anatomical anteroposterior was parallel to the load train. All tests were stopped at 10 % apparent strain.

To elucidate to what extent structural elements in the orthogonal direction to overload affect the mechanical integrity of cubes, all cubes were consecutively mechanically tested, to 10% apparent strain, in the direction orthogonal to the initial test. Thus, cubes initially assigned to SI were first overloaded in the superoinferior direction and then overloaded in the anteroposterior direction. This group will be referred to as S/A (Figure 4.1). Similarly, cubes initially assigned to AP were first overloaded in the anteroposterior direction and then overloaded in the superoinferior direction. This group will be referred to as A/S (Figure 4.1).

Due to the nature of the experiment described above, the standard platen test had to be used in place of the protocol suggested by Keaveny *et al* (10) for compression tests involving trabecular bone, as samples could not be embedded in brass endcaps.

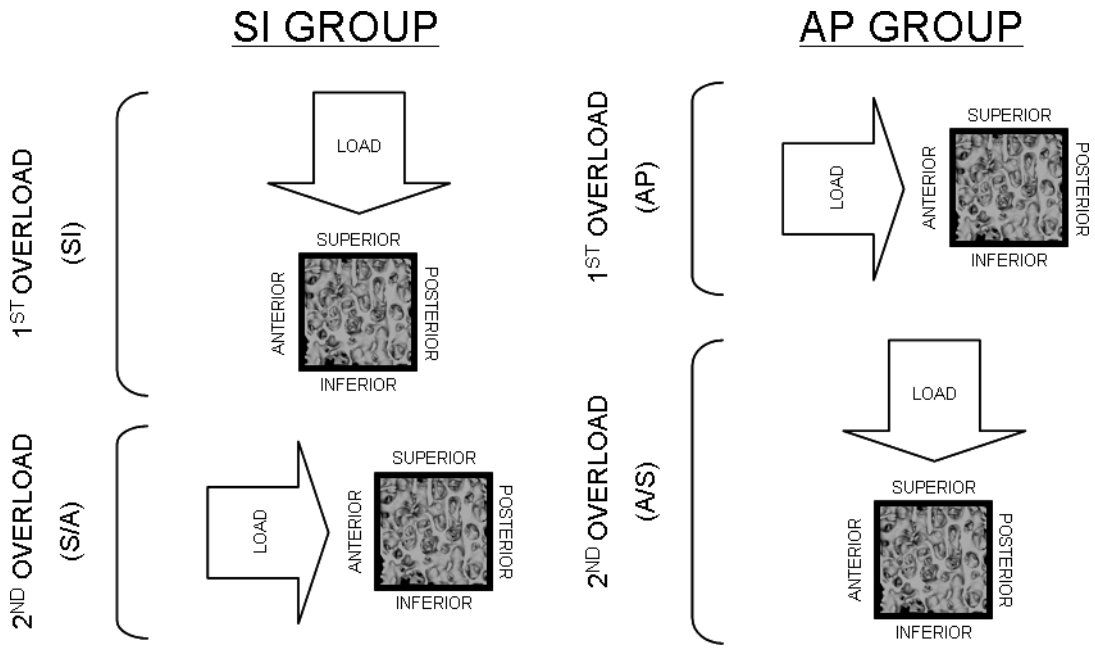

Figure 4.1 Schematic diagram of the overload experiments. For the SI group, the first overload was in the superoinferior direction (SI) followed by a second overload in the anteroposterior direction (S/A). For the AP group, the first overload was in the anteroposterior direction (AP) followed by a second overload in the superoinferior direction (A/S).

Following mechanical testing, cube dimensions and data from the load-deformation curves were used to compute the apparent ultimate failure stresses (UFS), apparent elastic moduli (E) and apparent toughness moduli (u) for both first and second overloads. Failure was defined as the point of maximal stress in the stress-strain curve, elastic modulus as the maximal slope of the elastic region of the stress-strain curve and modulus of toughness as the area under the stress-strain curve up to the point of failure (Chapter 2, Section 2.2.5). Machine compliance was tested using the protocol suggested by Turner and Burr (2001). No correction was applied for machine compliance as machine stiffness was found to be greater than the apparent stiffness of trabecular bone samples (22).

Regression analyses (least squares linear analyses) were used to test relationships between variables. Statistical differences between group means were tested using analysis of variance (ANOVA) and Student's t-test. Tukey's post-hoc test was used to identify groups that achieved significance from ANOVA. Statistical differences in regression line slopes were analyzed using analysis of covariance (ANCOVA). Statistical analyses were performed using both Matlab (The Mathworks) and SPSS (SPSS Inc.).

4.3 Results

4.3.1 Bone Architecture

No significant difference ($p > 0.05$) in BV/TV or architectural parameters was found between males and females. Similarly, no statistically significant difference ($p > 0.05$) was observed for mean BV/TV between pairwise combinations of cubes (Table 4.1), between cubes from T12/L1 and those from L4/L5 (Table 4.2) or between cubes assigned to SI and those assigned to AP testing groups (Table 4.3).

Statistically significant differences in SMI were identified between cubes from L4 vertebrae and those from both T12 ($p = 0.02$) and L1 ($p = 0.04$) vertebrae (Table 4.1). No statistically significant ($p > 0.05$) differences in architectural parameters were observed for any other pairwise combination of cubes. Significant differences were also found for mean Tb.N ($p = 0.03$), DA ($p = 0.01$), TBPf ($p = 0.04$) and SMI ($p = 0.01$) between T12/L1 and L4/L5 cubes (Table 4.2). However, no significant differences in architectural parameters were found between cubes assigned SI and those assigned to AP testing directions (Table 4.3).

Table 4.1 Mean ± standard deviation of μCT based BV/TV and architectural parameters of cubes from the spinal segments T12, L1, L4 and L5. P indicates significance of ANOVA across vertebral levels. Shaded boxes highlight significant ($p < 0.05$) differences, which were identified using Tukey's post-hoc analysis. #: $p = 0.02$ and *: $p = 0.04$

	T12 (N = 5)	L1 (N = 5)	L4 (N = 7)	L5 (N = 7)	P
BV/TV (%)	11.20 ± 1.81	11.27 ± 1.31	9.53 ± 1.09	11.26 ± 0.90	0.05
BS/BV (mm^2/mm^3)	19.40 ± 1.58	19.35 ± 0.60	20.02 ± 2.15	19.00 ± 2.17	0.78
BS/TV (mm^2/mm^3)	2.15 ± 0.20	2.18 ± 0.21	1.91 ± 0.28	2.14 ± 0.31	0.25
Tb.Th (μm)	180 ± 16	179 ± 9	184 ± 17	195 ± 26	0.47
Tb.Sp (μm)	1004 ± 104	1009 ± 97	1042 ± 132	989 ± 129	0.87
Tb.N (/mm)	0.62 ± 0.05	0.63 ± 0.06	0.52 ± 0.08	0.59 ± 0.10	0.09
DA (-)	2.37 ± 0.12	2.39 ± 0.10	2.15 ± 0.18	2.10 ± 0.35	0.08
TBPf (/mm)	5.19 ± 0.80	5.05 ± 0.33	6.37 ± 1.04	5.65 ± 0.97	0.06
SMI (-)	1.72 ± 0.14#	1.69 ± 0.11*	1.98 ± 0.16#*	1.88 ± 0.17	0.01
Conn.D ($/mm^3$)	2.20 ± 0.38	2.17 ± 0.45	2.13 ± 0.97	2.47 ± 1.21	0.89

Table 4.2 Mean ± standard deviation of μCT based BV/TV and architectural parameters of cubes from T12/L1 and L4/L5 pairings. P indicates significance of ANOVA between groups. Shaded boxes highlight significant ($p < 0.05$) differences.

	T12/L1 (N = 9)	L4/L5 (N = 15)	P
BV/TV (%)	11.44 ± 1.42	10.33 ± 1.29	0.06
BS/BV (mm^2/mm^3)	19.27 ± 1.14	19.57 ± 2.08	0.70
BS/TV (mm^2/mm^3)	2.19 ± 0.18	2.02 ± 0.30	0.12
Tb.Th (μm)	181 ± 12	187 ± 22	0.41
Tb.Sp (μm)	989 ± 83	1025 ± 129	0.47
Tb.N (/mm)	0.63 ± 0.05	0.56 ± 0.09	0.03
DA (-)	2.40 ± 0.10	2.13 ± 0.26	0.01
TBPf (/mm)	5.11 ± 0.61	5.96 ± 1.02	0.04
SMI (-)	1.71 ± 0.13	1.92 ± 0.17	0.01
Conn.D ($/mm^3$)	2.24 ± 0.37	2.25 ± 1.04	0.98

Table 4.3 Mean ± standard deviation of μCT based BV/TV and architectural parameters of cubes assigned to superoinferior (SI) and anteroposterior (AP) testing groups. P indicates significance of ANOVA between groups.

	SI (N = 12)	AP (N = 12)	P
BV/TV (%)	10.70 ± 1.47	10.79 ± 1.43	0.88
BS/BV (mm^2/mm^3)	19.59 ± 1.90	19.32 ± 1.68	0.71
BS/TV (mm^2/mm^3)	2.08 ± 0.25	2.08 ± 0.30	0.98
Tb.Th (μm)	183 ± 17	187 ± 21	0.59
Tb.Sp (μm)	1003 ± 117	1020 ± 114	0.72
Tb.N (/mm)	0.59 ± 0.07	0.58 ± 0.10	0.85
DA (-)	2.23 ± 0.24	2.23 ± 0.27	0.96
TBPf (/mm)	5.65 ± 1.04	5.62 ± 0.95	0.95
SMI (-)	1.83 ± 0.18	1.85 ± 0.19	0.82
Conn.D ($/mm^3$)	2.22 ± 0.73	2.28 ± 0.97	0.87

4.3.2 First Overload in the SI and AP Directions

Mean UFS, mean E and mean *u* were significantly ($p < 0.05$) greater in the SI group than in the AP group (76%, 84% and 61% respectively, Figure 4.2), with the expected strong positive linear relationship between UFS and E (8, 9) seen in both groups (Figure 4.3).

UFS was positively correlated to BV/TV in both SI and AP groups (Table 4.5 & Figures 4.5 & 4.6) while *u* was only significantly correlated to BV/TV in the SI group (Table 4.5). E was positively correlated to BV/TV in both SI ($E_{SI} = 0.16(BV/TV_{SI})^{2.5}$) and AP ($E_{AP} = 0.01(BV/TV_{AP})^{2.9}$) groups (Table 4.5). Different linear relationships between trabecular architecture and mechanics were observed in the two groups. In the SI group, significant relationships were observed between UFS and Tb.Th, while significant relationships were observed between *u* and both BS/TV and Tb.N. Significant relationships between E and BS/BV and E and Tb.Th were also observed (Table 4.5). In the AP group, significant relationships between UFS and the architectural parameters BS/TV, Tb.Sp, Tb.N and Conn.D were found. The same set of architectural parameters was also significantly correlated with E (Table 4.5). No significant relationships were identified between *u* and any of the architectural parameters in this group (Table 4.5).

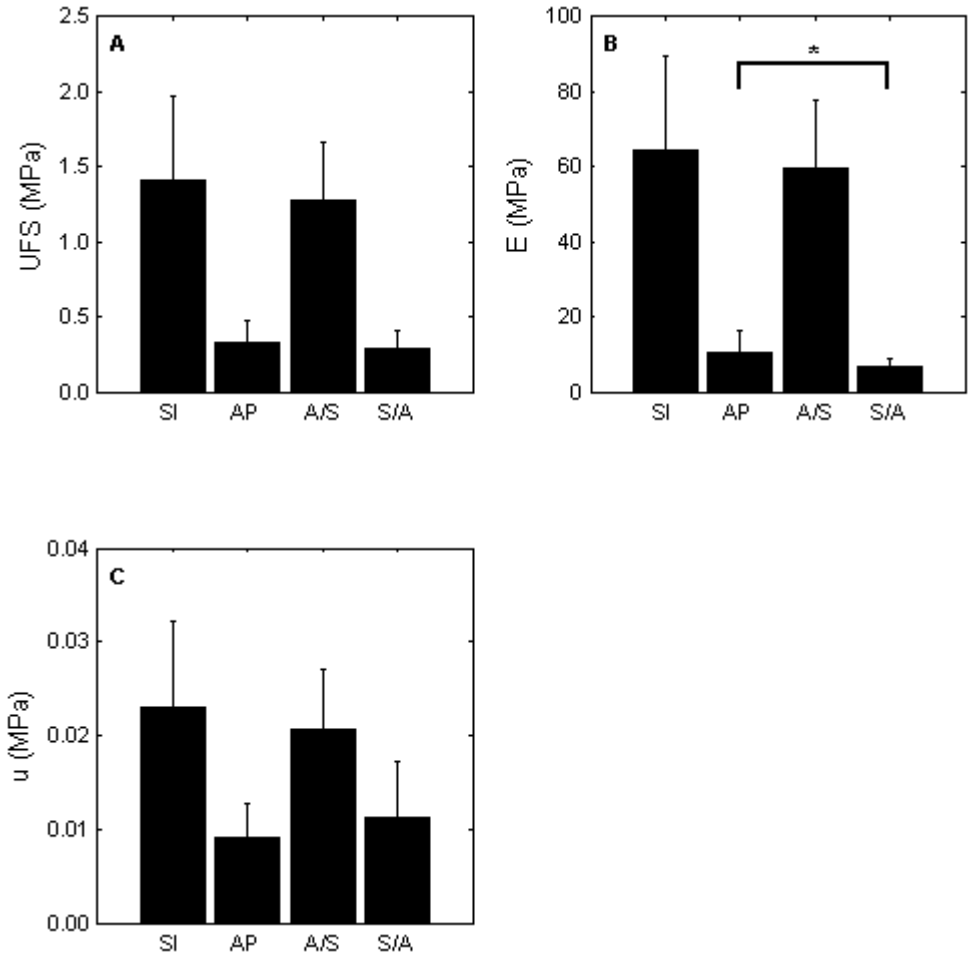

Figure 4.2 Bar graphs of mean + standard deviation of mechanical parameters: (A) UFS, (B) E and (C) u. SI represents cubes overloaded in superoinferior direction, AP represents cubes overloaded in the anteroposterior direction, A/S represents cubes overloaded in superoinferior direction following prior anteroposterior overload and S/A represents cubes overloaded in anteroposterior direction following prior superoinferior overload.

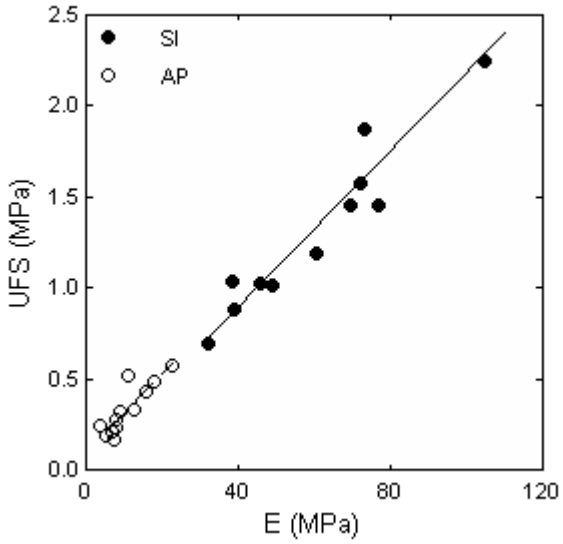

Figure 4.3 Relationship between UFS and E for the SI and AP mechanical tests. SI: UFS = 0.02E + 0.03, n = 12, r^2 = 0.95 and p < 0.001) and AP: UFS = 0.02E + 0.11 (n = 12, r^2 = 0.70 and p < 0.001). Regression line for SI data is shown as a solid line and regression line for AP data is shown as a broken line. No significant difference was observed between slopes of the regression lines (p = 0.99).

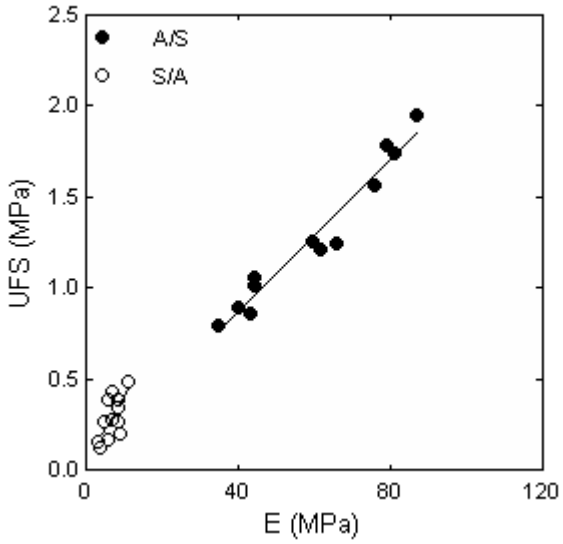

Figure 4.4 Linear relationships between UFS E for the second overload mechanical tests. A/S denotes superoinferior overload following prior anteroposterior overload and S/A anteroposterior overload following superoinferior overload. A/S: UFS = 0.02E + 0.03 (n = 12, r^2 = 0.92 and p < 0.001) and S/A: UFS = 0.03E + 0.07 (n = 12, r^2 = 0.49 and p = 0.01). Regression line for A/S data is shown as a solid line and regression line for S/A data is shown as a broken line. No significant difference was observed between slopes of the regression lines (p = 0.31).

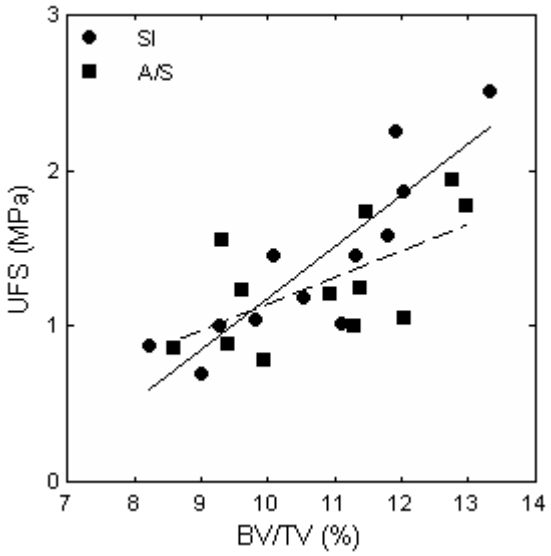

Figure 4.5 Linear relationships between UFS and BV/TV. SI indicates first overload results from the SI group and A/S indicates superoinferior overload results from samples with prior AP overload. $UFS_{SI} = 0.33BV/TV_{SI} - 2.16$ ($n_{SI} = 12$, $r^2_{SI} = 0.77$, $p < 0.001$) and $UFS_{A/S} = 0.17BV/TV_{A/S} - 0.55$, ($n_{A/S} = 12$, $r^2_{A/S} = 0.38$, $p < 0.04$). Regression line for SI data is shown as a solid line and regression line for A/S data is shown as a broken line. No significant difference was observed between slopes of the regression lines ($p = 0.08$).

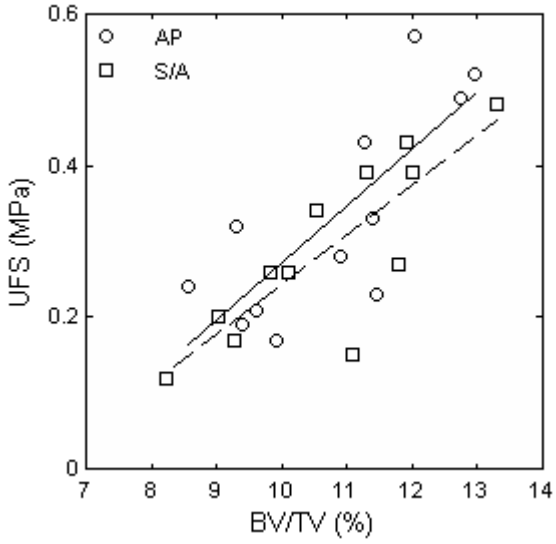

Figure 4.6 Relationship between UFS and BV/TV for anteroposterior mechanical tests. AP indicates first overload results from the AP group and S/A indicates anteroposterior overload results from samples with prior SI overload. $UFS_{AP} = 0.07BV/TV_{AP} – 0.41$, ($n_{AP} = 12$, $r^2_{AP} = 0.54$, $p < 0.007$); $UFS_{S/A} = 0.07BV/TV_{S/A} – 0.42$ ($n_{S/A} = 12$, $r^2_{S/A} = 0.67$, $p < 0.002$). Regression line for AP data is shown as a solid line and regression line for S/A data is shown as a broken line. No significant difference was observed between slopes of the regression lines ($p = 0.88$).

Table 4.5 Coefficient of determination (r^2) and significance between first overload mechanical parameters and μCT based BV/TV and architectural parameters for sample from SI and AP groups. Shaded boxes highlight significant ($p < 0.05$) relationships. ## indicates r^2 values for the power-law relationships: $E_{SI} = 0.16(BV/TV_{SI})^{2.5}$ and $E_{AP} = 0.01(BV/TV_{AP})^{2.9}$.

	SI (n = 12)			AP (n = 12)		
	UFS	E	*u*	UFS	E	*u*
BV/TV	0.77 p < 0.01	0.72## p < 0.05	0.79 p < 0.01	0.61 p < 0.01	0.51## p < 0.05	0.01 p = 0.72
BS/BV	0.28 p = 0.07	0.39 p = 0.03	0.19 p = 0.16	0.01 p = 0.73	0.02 p = 0.68	0.05 p = 0.47
BS/TV	0.31 p = 0.06	0.19 p = 0.16	0.42 p = 0.02	0.64 p < 0.01	0.59 p < 0.01	0.07 p = 0.41
Tb.Th	0.35 p = 0.04	0.43 p = 0.02	0.25 p = 0.10	0.00 p = 0.94	0.00 p = 0.99	0.02 p = 0.65
Tb.Sp	0.14 p = 0.23	0.06 p = 0.44	0.22 p = 0.13	0.69 p < 0.01	0.63 p < 0.01	0.15 p = 0.21
Tb.N	0.28 p = 0.08	0.18 p = 0.17	0.37 p = 0.03	0.46 p = 0.01	0.39 p = 0.03	0.04 p = 0.51
DA	0.01 p = 0.76	0.01 p = 0.77	0.01 p = 0.76	0.21 p = 0.13	0.29 p = 0.07	0.19 p = 0.16
TBPf	0.15 p = 0.21	0.21 p = 0.13	0.10 p = 0.31	0.00 p = 0.93	0.00 p = 1.00	0.16 p = 0.20
SMI	0.02 p = 0.64	0.03 p = 0.56	0.02 p = 0.70	0.01 p = 0.73	0.02 p = 0.66	0.09 p = 0.35
Conn.D	0.02 p = 0.67	0.00 p = 0.95	0.06 p = 0.43	0.43 p = 0.02	0.45 p = 0.02	0.11 p = 0.29

4.3.3 Second Overload in the Orthogonal Direction

Mean UFS, mean E and mean *u* were significantly greater in the A/S group compared to S/A group (77%, 89% and 46% respectively, Figure 4.4), similar to the relationship seen in the SI and AP groups. As expected (8, 9), in both A/S and S/A groups, UFS was positively correlated with E (Figure 4.4).

UFS showed significant and positive correlation with BV/TV in both A/S (Figure 4.5) and S/A groups (Figure 4.6) (Table 4.6). No significant difference was observed between the slope of the regression lines for SI and A/S ($p = 0.08$, Figure 4.5) or AP and S/A ($p = 0.88$, Figure 4.6) groups.

Relationships between the mechanical parameters and the architectural parameters for the 2nd overload tests showed a contrast to those seen in the 1st overload tests. In the A/S group, TBPf was the only architectural parameter to show a significant relationship with mechanical parameters (Table 4.6). In the S/A group, Tb.Th was the only architectural parameter to show a significant relationship to UFS, while both BS/TV and Tb.Th were identified as having significant relationships with *u*. None of the architectural parameters showed a significant correlation to E (Table 4.6).

Differences in superoinferior to anteroposterior mechanical properties (UFS, E and *u*) were greater than differences identified in superoinferior or anteroposterior mechanical properties after overloading in the orthogonal direction. Mechanical properties were significantly greater in SI than AP (UFS: 76%, E: 84% and *u*: 61%) and significantly greater in A/S than S/A (UFS: 77%, E: 89% and *u*: 46%) compared to the differences found between SI and A/S (UFS: 9%, E: 10% and *u*: 10%, $p > 0.05$) (Table 4.7) or between AP and S/A (UFS: 15% and *u* 20%, $p > 0.05$). However, mean E was significantly greater in the AP group than the S/A group ($p = 0.03$) (Table 4.8). No significant difference ($p = 0.89$) was found between the slopes of the regression lines between UFS and E for SI and A/S (Figure 4.7) or AP and S/A ($p = 0.24$) (Figure 4.8).

Table 4.6 Coefficient of determination (r^2) and significance between second overload mechanical parameters and μCT based BV/TV and architectural parameters. A/S represents cubes that underwent superoinferior overload following prior anteroposterior overload. S/A represents cubes that underwent anteroposterior overload following prior superoinferior overload. Shaded boxes highlight significant ($p < 0.05$) relationships. ## indicates values for the power-law relationships: $E_{A/S} = 0.34(BV/TV_{AP})^{1.3}$ and $E_{S/A} = 4.03(BV/TV_{SI})^{1.1}$.

	A/S (n = 12)			S/A (n = 12)		
	UFS	E	*u*	UFS	E	*u*
BV/TV	0.38 p = 0.03	0.21## p > 0.05	0.46 p = 0.02	0.67 p < 0.01	0.23## p > 0.05	0.77 p < 0.01
BS/BV	0.25 p = 0.10	0.25 p = 0.09	0.18 p = 0.18	0.29 p = 0.07	0.04 p = 0.55	0.26 p = 0.09
BS/TV	0.06 p = 0.45	0.01 p = 0.75	0.12 p = 0.27	0.25 p = 0.10	0.12 p = 0.26	0.36 p = 0.04
Tb.Th	0.05 p = 0.50	0.06 p = 0.46	0.02 p = 0.69	0.37 p = 0.04	0.05 p = 0.50	0.36 p = 0.04
Tb.Sp	0.00 p = 0.86	0.00 p = 0.88	0.02 p = 0.69	0.09 p = 0.34	0.03 p = 0.58	0.19 p = 0.15
Tb.N	0.10 p = 0.31	0.04 p = 0.56	0.19 p = 0.16	0.22 p = 0.13	0.13 p = 0.24	0.27 p = 0.08
DA	0.17 p = 0.18	0.26 p = 0.09	0.06 p = 0.43	0.03 p = 0.62	0.01 p = 0.74	0.00 p = 0.84
TBPf	0.42 p = 0.02	0.35 p = 0.04	0.41 p = 0.03	0.15 p = 0.22	0.04 p = 0.53	0.10 p = 0.33
SMI	0.28 p = 0.08	0.20 p = 0.14	0.33 p = 0.05	0.02 p = 0.65	0.04 p = 0.53	0.00 p = 0.98
Conn.D	0.02 p = 0.65	0.06 p = 0.45	0.00 p = 0.90	0.02 p = 0.70	0.04 p = 0.51	0.06 p = 0.43

Table 4.7 Mean ± standard deviation and percent difference (% DIFF.) from mechanical tests in the superoinferior direction. SI indicates first overload results from the SI group and A/S indicates superoinferior overload results from AP group with prior AP overload. P indicates significance of Student's paired t-test between the two groups.

	SI	A/S	% DIFF.	P
UFS (MPa)	1.41 ± 0.6	1.28 ± 0.4	9	0.50
E (MPa)	66.9 ± 27.2	60.4 ± 18.5	10	0.49
u (MPa)	0.023 ± 0.009	0.021 ± 0.006	10	0.50

Table 4.8 Mean ± standard deviation and percent difference (% DIFF.) from mechanical tests in the anteroposterior direction. AP indicates first overload results from the AP group and S/A indicates anteroposterior overload results from SI group with prior SI overload. P indicates significance of Student's paired t-test between the two groups. Shaded boxes highlight significant ($p < 0.05$) differences.

	AP	S/A	% DIFF.	P
UFS (MPa)	0.34 ± 0.1	0.29 ± 0.1	15	0.32
E (MPa)	10.4 ± 5.6	6.8 ± 2.4	35	0.03
u (MPa)	0.009 ± 0.004	0.011 ± 0.006	20	0.25

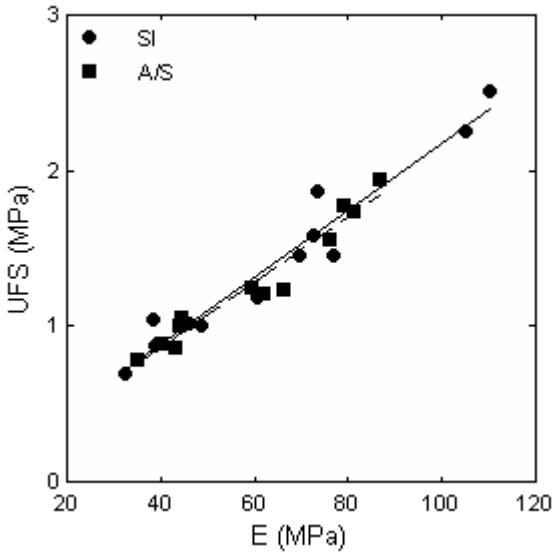

Figure 4.7 Relationship between UFS and E for superoinferior mechanical tests. SI indicates first overload results from the SI group and A/S indicates superoinferior overload results from samples with prior AP overload. $UFS_{SI} = 0.020E_{SI} + 0.07$ ($n_{SI} = 12$, $r^2_{SI} = 0.95$, $p < 0.001$); $UFS_{A/S} = 0.020E_{A/S} + 0.05$ ($n_{A/S} = 12$, $r^2_{A/S} = 0.92$, $p < 0.001$). Regression line for SI data is shown as a solid line and regression line for A/S data is shown as a broken line. No significant difference was observed between slopes of the regression lines ($p = 0.89$).

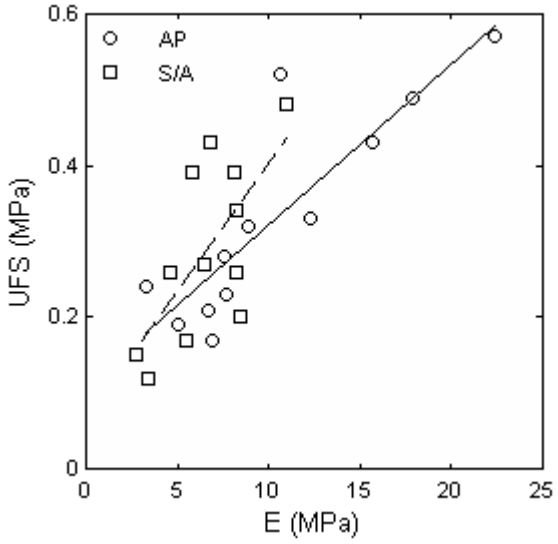

Figure 4.8 Relationship between UFS and E for anteroposterior mechanical tests. AP indicates first overload results from the AP group and S/A indicates anteroposterior overload results from samples with prior SI overload. $UFS_{AP} = 0.020E_{AP} + 0.13$ ($n_{AP} = 12$, $r^2_{AP} = 0.70$, $p < 0.001$); $UFS_{S/A} = 0.034E_{S/A} + 0.06$ ($n_{S/A} = 12$, $r^2_{S/A} = 0.48$, $p < 0.02$). Regression line for AP data is shown as a solid line and regression line for S/A data is shown as a broken line. No significant difference was observed between slopes of the regression lines ($p = 0.24$).

4.4 Discussion

The mean magnitudes of UFS and E for the SI and AP groups were similar to those reported by Mosekilde *et al* (1985) (18) and others (7, 16, 17), with slight differences likely to be due to difference in cohort age and test protocols. In addition, relationships between bone volume fraction and mechanical parameters for these groups were similar to those reported by others (7, 8, 17).

A number of investigators (5, 17, 18) have demonstrated the presence of mechanical anisotropy in vertebral trabecular bone and results from this study complement those findings. Superoinferior mechanical properties were greater than anteroposterior mechanical properties, in spite of the fact that there was no significant difference in global BV/TV or global architecture between cubes randomly assigned to the SI and AP groups. Even after overload in the orthogonal direction, the UFS, E and *u* were greater in magnitude for the A/S group than the S/A group. Hence, the mechanical anisotropy observed in the present study and by others (5, 17, 18) was still present after the trabecular structure was mechanically overloaded in the orthogonal direction (Figure 4.2). Moreover, the mechanical anisotropy was greater when comparing SI with AP or A/S with S/A, than differences found before and after overload in the orthogonal direction. Thus, mechanical anisotropy resulted in greater differences between superoinferior and anteroposterior mechanical properties compared to differences resulting from overloading the structure in the orthogonal direction.

No significant difference was found between the SI and A/S groups in terms of mean UFS and mean *u*. Similarly, no significant difference was found between the AP and S/A groups in terms of mean UFS and mean *u*. In contrast, E was found to be 35% less in the S/A group than the AP group. No such difference was found between SI and A/S groups. These results suggest that overloading in the anteroposterior direction had little effect on the superoinferior mechanical integrity, while overloading in the superoinferior direction had the effect of reducing the apparent elastic modulus in the anteroposterior direction. This combined with the observation that apparent ultimate failure stress was not significantly different from the cubes mechanically tested under first overload, suggests the energy required to cause failure, that is, modulus of toughness, is determined by strain to failure. This property acts as a protection mechanism for the maintenance of a functional trabecular structure.

These findings are supported by the work of Fyhrie and Schaffler (1994) (4) and others (11, 12, 14, 24, 25). Fyhrie and Schaffler took cubes of vertebral trabecular bone and performed uni-axial mechanical testing past the point of failure. Samples were then analyzed both macro- and microscopically. They found that macroscopic damage from superoinferior testing resulted in little or no structural damage to superoinferior trabecular elements with virtually all damage restricted to horizontal trabecular elements transverse to the superoinferior loading direction. These horizontal elements were found to have failed by [1] “fracturing off at the base from connection to a vertical trabecula”, [2] “split along the axis” or [3] “broken in the middle”. Microscopic examination highlighted that superoinferior elements were grossly intact but did “sustain internal matrix microdamage”. They suggested that these failure mechanisms allow trabecular bone to recover its initial form even though the apparent elastic modulus of the structure would be diminished. They suggest this pattern of damage is a mechanism that may allow the trabecular bone to heal and restore close to original function. Fyhrie and Schaffler’s (1994) (4) observations go part way to explaining why, in the present study, a 35% decrease in apparent elastic modulus was noted in cubes overloaded in the superoinferior direction then overloaded in the anteroposterior direction

(S/A group). In the present study, even though no micro- or macroscopic examinations were carried out, the range and magnitude of UFS in combination with the fact that mechanical tests were overload tests, suggests that the damage sustained to the trabecular structure would have been similar to that observed by Fyhrie and Schaffler.

Fyhrie and Schaffler did not look at the affect of transverse element failure on longitudinal elements. In this case, the present study's results suggest that the failure mechanism for anteroposterior compression differs from that of superoinferior compression. This is further supported by the observations that mechanical anisotropy differences, that is, superoinferior versus anteroposterior, were greater than differences induced through overloading in the orthogonal direction. This highlights a structural property that may have significant influence on trabecular bone damage mechanics.

Keaveny *et al* (1994) (11) carried out post-failure tests on bovine proximal tibia trabecular bone, where reduced-section cylinders of trabecular bone were tested to different strains (1%, 2.5%, 4% and 5.5%), unloaded to 0% strain and reloaded to 9% strain. They found that the elastic modulus was reduced in all tests, whereas strains of $\geq$ 2.5% were required to produce reductions in strength. In general their findings suggest that compromising the trabecular structure leads to a greater reduction in the elastic modulus than strength. Comparable findings were also demonstrated in human vertebral trabecular bone (12) and in the whole vertebral body (14). Similar to the hypotheses of Fyhrie and Schaffler (1994) (4), Keaveny *et al* suggest that trabecular bone has ultra-structural material properties that aid the trabecular structure in maintaining function and healing subsequent to damage.

Wang *et al* (2005) (24) mechanically tested samples of bovine proximal tibia bone by compressive overloading followed by torsional overloading. In a subsequent study, Wang *et al* (25) mechanically tested similar bovine proximal tibia samples by torsional overloading followed by compressive overloading. In each study a number of microdamage variables were measured. In comparing the two studies, Wang *et al* concluded that the percentage of the original microcracks that propagated due to compressive overloading followed by torsional overloading were significantly greater than those from torsional overloading followed by compressive overloading (25). Although the type of bone and the modes of loading differ to the present study, Wang *et al* provide insight into the underlying mechanisms of trabecular bone damage properties and further support the notion that material properties at the ultra-structural level help to dissipate energy and increase the energy required to cause failure (3, 24).

Taken together, the findings of these previous studies and the present study suggest a complex relationship between the failure mechanisms and mechanical roles of longitudinal and transverse elements of the vertebral body. One explanation of the observations is that, in addition to the mechanical support role of the transverse elements, they may have a significant role in the dissipation of energy during trauma to the trabecular structure. In effect, they may act as sacrificial elements in a crumple-zone allowing energy to be dissipated away from the main longitudinal elements, thereby minimizing damage to these primary elements, analogous to the crumple-zones in modern vehicles. In the context of aging and osteoporosis, one could speculate that the loss or reduction in the thickness of these transverse elements (1, 15) would result in the trabecular structure having less protection and thus resulting in more significant damage during trauma, which, if not given the appropriate time and conditions to heal, would result in further damage leading to failure.

Unlike previous studies investigating trabecular bone damage (4, 11, 12, 14), here μCT based model-independent architectural parameters were also measured. Results comparing architectural parameters with SI and AP group mechanics showed similar results to those found by other investigators (2, 21, 23). In the SI group, significant relationships were observed between UFS, E and *u* and a number of architectural parameters, including BS/BV, BS/TV, Tb.Th and Tb.N. In contrast, architectural parameters showed a different contribution to the AP group mechanical properties, where UFS and E showed significant relationships to BS/TV, Tb.Sp, Tb.N and Conn.D, while no significant relationships were identified between *u* and any architectural parameters. These results highlight that in anteroposterior loading, the spatial arrangement and connectivity of the trabecular structures play a more significant role than just Tb.Th. This is in contrast to longitudinal loading and so further supports the notion that there are differences between longitudinal and anteroposterior element response to mechanical loading.

With A/S and S/A groups, the relationships between mechanical parameters and architecture were different to that seen for the SI and AP groups. Significant relationships were found with TBPf,

Tb.Th and BS/TV for A/S and S/A groups. The relationship between UFS and *u* with BV/TV was weaker for the A/S tests than the first overload mechanical results of the SI group, yet for S/A tests this relationship was even stronger than that seen for the AP group. The fact that no statistically significant differences were found between A/S and SI groups for mean UFS, mean E and mean *u*, yet the relationship between architectural and mechanical parameters were different, indicates that the structural basis for the relationship must have changed. This, together with the observation that a significant 35% reduction in E was found between S/A and AP groups, also indicates differences in mechanical response between anteroposterior compared to longitudinal directions.

Power-law relationships between modulus of elasticity and volume fraction were presented as opposed to linear relationships due to the fact that there is a general consensus that the relationship between volume fraction and elastic modulus is a power-law relationship (20, 22). This is attributed to observations that small increases in porosity (which is related to volume fraction) can result in larger reductions in elastic modulus (22). In the present study, power-law exponents ranged from 1.1 to 2.9 and were well within the range found in the literature (20, 22) .

Work by Keaveny *et al* (1997) (10) suggests that the platen compression test has inherent systemic and random errors that contribute to underestimation of mechanical properties. The protocol presented by Keaveny *et al* includes embedding samples in brass endcaps. In the current investigation, each sample was tested twice, once in each of the two directions. This precludes the use of endcaps. Also, while the suggested protocol is of importance in determining absolute values, the systemic errors addressed by the protocol of Keaveny *et al* are not critical in the current study since relative differences are examined. As such, the mechanical testing protocol presented is valid. In addition, cube dimensions were measured once prior to initial mechanical testing. These cube dimensions were then used throughout the experiment, even though mechanical testing would have induced small changes to the cube dimensions. Given the observations of Fyhrie and Schaffler (1994) (4) that, on average, after release of compressive load, at least 96% of the original height of

vertebral cubes samples compressed to 85% of their original height is regained, errors induced by the use of the original cube dimensions were considered negligible.

Given the present study's small sample size, a certain degree of uncertainty resulting from the distribution of samples from different vertebral levels was expected. Slight differences in mechanical properties were expected between vertebral levels. However, the analyses suggested the spread was even. Architectural differences identified included differences in Tb.N, DA, TBPf and SMI between T12/L1 and L4/L5 cubes. However, as cubes from T12/L1 and L4/L5 were distributed between SI and AP groups, variability was also distributed between groups. Similarly, variability introduced by differences in SMI between T12 and L4 and L1 and L4 were also distributed between the SI and AP groups.

In summary, this study has highlighted differences between the longitudinal and anteroposterior elements of vertebral trabecular bone. Differences in mechanical response were found between superoinferior and anteroposterior directions after overload in the orthogonal direction. The mechanical anisotropy of vertebral trabecular bone far exceeded any differences induced by overloading the structure in the orthogonal direction. This in itself indicates that mechanical anisotropy is an important property. Observations suggest that the trabecular structure has properties that minimize loss of apparent toughness, perhaps through energy dissipating sacrificial structures transverse to the primary loading direction. Underlying relationships between trabecular architecture and mechanical properties were also found to be different for the two directions with global architectural parameters not providing insight into mechanical anisotropy phenomena that was observed.

Given these findings, non-invasive measurement of structural anisotropy could provide important diagnostic information about the integrity of trabecular bone. The next chapters will look at techniques for assessing structural anisotropy using non-invasive methodologies.

References

1. Atkinson, P. J. Variation in trabecular structure of vertebrae with age. Calcif Tissue Res 1:24-32; 1967.
2. Cendre, E., Mitton, D., Roux, J. P., Arlot, M. E., Duboeuf, F., Burt-Pichat, B., Rumelhart, C., Peix, G., and Meunier, P. J. High-resolution computed tomography for architectural characterization of human lumbar cancellous bone: relationships with histomorphometry and biomechanics. Osteoporos Int 10:353-60; 1999.
3. Fazzalari, N. L., Forwood, M. R., Smith, K., Manthey, B. A., and Herreen, P. Assessment of cancellous bone quality in severe osteoarthrosis: bone mineral density, mechanics, and microdamage. Bone 22:381-8; 1998.
4. Fyhrie, D. P., and Schaffler, M. B. Failure mechanisms in human vertebral cancellous bone. Bone 15:105-9; 1994.
5. Galante, J., Rostoker, W., and Ray, R. D. Physical properties of trabecular bone. Calcif Tissue Res 5:236-46; 1970.
6. Hansson, T., and Roos, B. Microcalluses of the trabeculae in lumbar vertebrae and their relation to the bone mineral content. Spine 6:375-80; 1981.
7. Hansson, T. H., Keller, T. S., and Panjabi, M. M. A study of the compressive properties of lumbar vertebral trabeculae: effects of tissue characteristics. Spine 12:56-62; 1987.
8. Keaveny, T. M., and Hayes, W. C. A 20-year perspective on the mechanical properties of trabecular bone. J Biomech Eng 115:534-42; 1993.
9. Keaveny, T. M., Morgan, E. F., Niebur, G. L., and Yeh, O. C. Biomechanics of trabecular bone. Annu Rev Biomed Eng 3:307-33; 2001.
10. Keaveny, T. M., Pinilla, T. P., Crawford, R. P., Kopperdahl, D. L., and Lou, A. Systematic and random errors in compression testing of trabecular bone. J Orthop Res 15:101-10; 1997.
11. Keaveny, T. M., Wachtel, E. F., Guo, X. E., and Hayes, W. C. Mechanical behavior of damaged trabecular bone. J Biomech 27:1309-18; 1994.
12. Keaveny, T. M., Wachtel, E. F., and Kopperdahl, D. L. Mechanical behavior of human trabecular bone after overloading. J Orthop Res 17:346-53; 1999.
13. Kitahara, H. [Morphological observations on trabecular microfractures in the lumbar vertebrae (author's transl)]. Nippon Seikeigeka Gakkai Zasshi 54:449-60; 1980.
14. Kopperdahl, D. L., Pearlman, J. L., and Keaveny, T. M. Biomechanical consequences of an isolated overload on the human vertebral body. J Orthop Res 18:685-90; 2000.
15. Mosekilde, L. Age-related changes in vertebral trabecular bone architecture--assessed by a new method. Bone 9:247-50; 1988.
16. Mosekilde, L. Normal vertebral body size and compressive strength: relations to age and to vertebral and iliac trabecular bone compressive strength. Bone 7:207-12; 1986.
17. Mosekilde, L., and Danielsen, C. C. Biomechanical competence of vertebral trabecular bone in relation to ash density and age in normal individuals. Bone 8:79-85; 1987.
18. Mosekilde, L., and Viidik, A. Correlation between the compressive strength of iliac and vertebral trabecular bone in normal individuals. Bone 6:291-5; 1985.
19. Nguyen, T. V., Center, J. R., and Eisman, J. A. Osteoporosis: underrated, underdiagnosed and undertreated. Med J Aust 180:S18-22; 2004.
20. Rice, J. C., Cowin, S. C., and Bowman, J. A. On the dependence of the elasticity and strength of cancellous bone on apparent density. J Biomech 21:155-68; 1988.
21. Thomsen, J. S., Ebbesen, E. N., and Mosekilde, L. Predicting human vertebral bone strength by vertebral static histomorphometry. Bone 30:502-8; 2002.
22. Turner, C. H and Burr, D. B. Experimental Techniques for Bone Mechanics. In: S. C. Cowin (ed.), Bone Mechanics Handbook, pp. 7/1 - 7/35, CRC Press, 2001.
23. Ulrich, D., van Rietbergen, B., Laib, A., and Ruegsegger, P. The ability of three-dimensional structural indices to reflect mechanical aspects of trabecular bone. Bone 25:55-60; 1999.
24. Wang, X., Guyette, J., Liu, X., Roeder, R. K., and Niebur, G. L. Axial-shear interaction effects on microdamage in bovine tibial trabecular bone. Eur J Morphol 42:61-70; 2005.
25. Wang, X., and Niebur, G. L. Microdamage propagation in trabecular bone due to changes in loading mode. J Biomech 39:781-90; 2006.